Applied Catalysis B: Environmental 129 (2013) 202–213

Contents lists available at SciVerse ScienceDirect

Applied Catalysis B: Environmental

journal homepage: www.elsevier.com/locate/apcatb

Study on the effect of metal types in (Me)-Al-MCM-41 on the mesoporous structure and catalytic behavior during the vapor-catalyzed co-pyrolysis of pubescens and LDPE

Wen-Wu Liu[a,b], Chang-Wei Hu[a,*], Yu Yang[a], Dong-Mei Tong[a], Liang-Fang Zhu[a], Rui-Nan Zhang[a], Bo-Han Zhao[a]

[a] Key Laboratory of Green Chemistry and Technology, Minister of Education, College of Chemistry, Sichuan University, 29 Wangjiang Road, Chengdu, 610064, PR China
[b] Yibin University, 8 Jiusheng Road, Yibin, 644000, PR China

ARTICLE INFO

Article history:
Received 23 April 2012
Received in revised form 3 September 2012
Accepted 4 September 2012
Available online 12 September 2012

Keywords:
Co-pyrolysis
Alkanisation
Aromatization
(Me)-Al-MCM-41
Synergistic effect

ABSTRACT

The catalysts (Me)-Al-MCM-41 (Me = Ni, Pd and their combination) were synthesized hydrothermally, characterized with XRD, BET, NH_3-TPD, SEM, TEM, XPS, H_2-TPR, chemisorption of hydrogen, and tested by experiments of co-pyrolysis of pubescens and LDPE under vapor-catalyzed condition. Characterization results suggested that the synthesis of Al-MCM-41 was successful, but the introduction of Me into Al-MCM-41 caused some changes in structure of catalyst to a certain degree, resulting in significant changes in their properties and catalytic behavior. The results obtained from vapor-catalyzed co-pyrolysis over these catalysts showed that there were some interactions between the intermediate species from the co-pyrolysis, as the relative content of aromatics in oil was high, whereas that of phenol in corresponding aqua was low, and vice versa. The type of metal in catalysts was of more importance than the metal siting. Moreover, all catalysts except Ni-Pd-Al-MCM-41 exerted strong effect of alkanisation on the primary intermediate species from the pyrolysis of LDPE, which demonstrated that the pore architecture of parent Al-MCM-41 and (Me)-Al-MCM-41 containing single Me strongly favored the reactions in relation to alkanisation; on the contrary, Ni-Pd-Al-MCM-41 exerted a strong effect of dehydrogenation on those primary intermediate species. More importantly, the synergistic effect on producing hydrogen, based on the 61.8 vol.% of H_2 in gaseous mixture, indicated that the combination of Ni and Pd in (Me)-Al-MCM-41 might bring about a novel performance during the vapor-catalyzed co-pyrolysis of biomass and plastics. It was predicted that Ni-Pd-Al-MCM-41 might play its special application in development of hydrogen energy, exploitation and utilization of biomass as well as municipal solid waste (MSW) such as waste plastics, etc. The major schemes of reactions involved in the vapor-catalyzed co-pyrolysis had been proposed.

1. Introduction

At present the increasing demand for fossil resources has been confronted with some severe problems such as shortage and environmental pollution, so various recycling methods of waste plastics were studied to reproduce fuel oil or valuable chemicals. Catalytic pyrolysis of plastics is considered most promising because the catalysts applied can activate the carbocationic mechanisms for cracking the primary intermediate species and the subsequent reactions [1–4].

Biomass is a renewable energy resource, and is considered cheap, promising and available in abundance. In general, the liquid from thermal pyrolysis of biomass could not be directly used as fuel, due to its defects such as high content of oxygen and water, less stability and less miscibility in conventional fuel, so various catalysts have also been introduced into the pyrolysis of biomass to improve the quality of bio-fuel as well as chemicals [5,6].

In view of the co-existence of biomass and plastics in municipal solid waste (MSW), their co-pyrolysis seems to be an attractive way for both environmental protection and sustainable development. Some works on the co-conversion assumed that the co-pyrolysis of plastics and biomass could allow possible chemical interactions between their cracking intermediate species, resulting in some positive changes in the yield and quality of the final products [7–12].

MCM-41, one of the typical representatives of the mesoporous molecular sieve, possesses a hexagonal array of uniform

* Corresponding author. Tel.: +86 28 85411105; fax: +86 28 85411105.
E-mail addresses: Changweihu@scu.edu.cn, gchem@scu.edu.cn (C.-W. Hu).

0926-3373/$ – see front matter © 2012 Elsevier B.V. All rights reserved.
http://dx.doi.org/10.1016/j.apcatb.2012.09.002

mesopores, and exhibits high surface area and mild-to-moderate acidity [13]. A combination of the specific porosity with the catalytic active sites leads to its wide application to novel catalysts or catalyst carriers. For example, a series of mono/bimetallic ions modified MCM-41 catalysts had been used as catalysts for partial oxidation of hydrocarbons under mild conditions [14,15]; the mesoporous aluminosilicates Al-MCM-41 as well as single metal-containing Me-Al-MCM-41 was considered to be very beneficial with respect to the catalytic pyrolysis of biomass or plastics [16–24,2]. Antonakou et al. [16] had applied three kinds of Al-MCM-41 with different Si/Al ratio and three single metal-containing samples of Me-Al-MCM-41 to the in situ catalytic upgrading of vapors from the pyrolysis of biomass. They found that all catalysts were active in increasing the amount of phenolic compounds, and Fe/Cu-Al-MCM-41 were the best metal containing catalysts in terms of phenols production; a low Si/Al ratio was found to have a positive effect on product yields and composition; furthermore, these results were contributed to the large pore dimensions and the mild-to-moderate acidity. Adam et al. [17] had upgraded the pyrolysis vapors of spruce wood by four different Al-MCM-41 type catalysts with the help of on-line Py-GC/MS. Their results showed that all catalysts repressed to a great extent the formation of levoglucosan, while increased the yield of acetic acid and that of furans; lowered that of higher molecular mass phenols. Furthermore, the effect of MCM-41 catalyst seemed to be related to the size of the catalyst pores, yet the Cu modified catalyst performed similarly to the catalyst with enlarged pore size in converting the pyrolysis vapors of wood. Adam et al. [18] had also investigated the effect of seven mesoporous catalysts on the in situ upgrading of biomass vapors in a fixed bed reactor and achieved similar results to that in Ref. [16]. Chaianansutcharit et al. [19] had studied the degradations of PP and PE over pure hexagonal mesoporous silica (HMS) and aluminum-containing hexagonal mesoporous silica (Al-HMS) in a fixed bed reactor. They found that HMS had no catalytic activity for degradation of plastics in liquid-phase-contact (LPC) mode or vapor-phase-contact (VPC) mode, while Al-HMS exhibited good performance in cracking heavy molecular weight hydrocarbons into light hydrocarbons, resulting in high liquid yields and less coke deposits produced in LPC reaction and more gaseous products in VPC reaction. Nilsen et al. [20] had fully characterized four (Me)-Al-MCM-41 catalysts in order to obtain structural information about the local metal surroundings. Their results showed that the metal sitings were different in these materials, and the type of metal was of more importance than the metal siting.

In this work, a parent Al-MCM-41 and Me-Al-MCM-41 (Me being Ni, Pd and their combination ($n_{Ni} = n_{Pd}$)) were hydrothermally synthesized as described in Ref. [18]. These catalysts were under study in the co-pyrolysis of pubescens and LDPE in order to investigate the effect of pore size, acidity and type of metal, etc. on the yields and compositions of products.

2. Experimental

2.1. Raw materials

Pubescens is collected from the Sichuan Province of China. The air-dried pubescens is smashed into powder and then screened to give fraction with the particle size of 360 μm. Low density polyethylene (LDPE) with a density of 0.9 g/cm^3 is obtained from Lanzhou Petrochemical Corporation (Lanzhou, China).

$C_{14}H_{29}(Me)_3NBr$ is used as surfactant. All reagents applied in this work are of analytical grade.

2.2. Catalyst preparation

2.2.1. Al-MCM-41

Molar composition: 1Si:0.06Al:0.4C_{14}:68H_2O (C_{14}: the surfactant).

Al-MCM-41 is prepared in the following steps:

1. The surfactant ($C_{14}H_{29}(Me)_3NBr$, 15 g) is dissolved in water (95 g) with stirring at 30 °C.
2. The aluminum source, sodium-aluminate (0.43 g) is added and the solution is stirred overnight.
3. Silica source, $Na_2SiO_3{\cdot}9H_2O$ (25 g), sulfuric acid (10%, 5.6 g) and water (15 g) are added, and the solution is stirred for 30 min. Then the pH is adjusted to ~10 with 50% sulfuric acid.
4. The solution is filled in a Teflon-flask, heated at 125 °C for 6 days, washed with distilled water until pH 5. The white product is dried for 4 h at room temperature in vacuum, and then is dried in oven at 100 °C overnight.
5. The white product obtained in Step 4 is heated at 560 °C [13,20] (heating rate is 3 °C/min) for 1 h under nitrogen atmosphere (flow rate is 60 ml/min), then nitrogen is replaced with air (conditions: 60 ml/min, 560 °C, and 6 h). The heating is stopped and the final product is cooled under nitrogen atmosphere overnight.

2.2.2. Me-Al-MCM-41 (the molar composition: 1Si:0.06Al:0.1 Me:0.2C_{14}:64H_2O)

For Me-Al-MCM-41 catalysts, the preparation of Ni-Pd-Al-MCM-41 is taken as an example, as others are similar to this.

Molar composition: 1Si:0.06Al:0.05Ni:0.05Pd:0.2C_{14}:64H_2O.

1. The surfactant ($C_{14}H_{29}(Me)_3NBr$, 7.1 g) is dissolved in water (50 g) with stirring for 1 h at 30 °C.
2. Sodium-aluminate (0.45 g) is dissolved in water (40 g) and then sulfuric acid (95%, 1.5 g) is added to the solution, which is stirred for 45 min. Ni $(NO_3)_2{\cdot}6H_2O$ (2.6 g) is added to the solution of aluminium, and stirred for 1 h. Then $PdCl_2$ (1.58 g) is added with stirring for another 1 h.
3. The solution obtained in Step 2 is added dropwise to the solution of template and stirred for 1 h.
4. Silica source, $Na_2SiO_3{\cdot}9H_2O$ (25 g) is dissolved in water (35 g) and stirred for 50 min before it is added dropwise to the solution described above and stirred for 2 h. Then the pH is adjusted to ~10 with 50% sulfuric acid.
5. Similar to Step 4 in preparation of Al-MCM-41, and the product is light-brown.
6. The brown product obtained in Step 5 is heated, temperature programming, under nitrogen atmosphere (60 ml/min) to 200 °C (20 °C/min), then heated to 300 °C (50 °C/min) and kept for 0.5 h, and then nitrogen is replaced with air (60 ml/min) and kept for 1 h, and heated to 560 °C (5 °C/min) with a retention time of 6 h. Then heating is stopped and the final product is cooled under nitrogen atmosphere overnight.

2.3. Experimental unit and procedure

In this work, the experimental unit, procedures are similar to our previous work [25]. The co-pyrolysis experiments are carried out in a fixed bed reactor. The reactor is composed of two glass tubes. The bottom of inner tube is sealed for acting as the pyrolytic cell. A fixed catalyst bed made of copper gauze (200 meshes) is designed and placed just under the inner tube to realize the catalytic effect of (Me)-Al-MCM-41 on the secondary reactions of primary intermediate species from the pyrolytic cell. The distance between the outlet of the inner tube and the fixed catalyst bed is 16 cm.

Co-pyrolysis experiments are performed at 470–450 °C for 2.5 h under N_2 atmosphere. 2 g sample of pubescens and 8 g sample of LDPE is mixed and then pyrolyzed with a heating rate of 10 K/min, the temperature of each zone of the furnace is measured by thermocouples. The volatiles from the pyrolytic cell initially ascend to the outlet of the inner tube, and then are swept down by nitrogen gas with a flow rate of 50 mL/min. 0.5 g sample of catalyst (Me)-Al-MCM-41 is placed on the fixed catalyst bed for the vapor-phase-contact reaction. The liquid products are collected in an ice trap (0 °C), and the gaseous products are collected for analysis.

2.4. Product analysis

The liquid products and the residue are weighted directly. The yield of liquid product, the percentage of residue and that of gas plus losses are calculated as follows:

$$\text{Yield of liquid (L, wt.\%)} = \left(\frac{\text{weight of liquid}}{\text{weight of reactants}}\right) \times 100 \quad (1)$$

$$\text{Percentage of residue (R, wt.\%)} = \left[\frac{\text{weight of remaining in the degradation reactor-weight of catalyst}}{\text{weight of reactants}}\right] \times 100 \quad (2)$$

$$\text{Percentage of gases (G, wt.\%) (plus losses)} = 100 - (\text{L} + \text{R}) \quad (3)$$

The liquid is separated with a separating funnel, the upper phase is defined as "oil" (mainly from the pyrolysis of LDPE), and another phase is called "aqua" (mainly from the pyrolysis of pubescens). The yield of oil and that of aqua are calculated as follows:

$$\text{Yield of oil (O, wt.\%)} = \left(\frac{\text{weight of oil}}{\text{weight of reactants}}\right) \times 100 \quad (4)$$

$$\text{Yield of aqua (A, wt.\%)} = \left(\frac{\text{weight of aqua}}{\text{weight of reactants}}\right) \times 100 \quad (5)$$

The composition and relative content of the liquid products are analyzed using Agilent 6890 series GC system supplied with 5973 mass selective detector (USA). The GC program is: injector temperature, 250 °C; column temperature, 100–230 °C (running in temperature programming); carrier gas, helium; split ratio, 10:1; total flow rate, 16 mL/min.

The gases are collected and analyzed by a thermal conductivity detector in temperature programming with separation by gas chromatography (SP-6800A) using a column packed with porapak Q (2 m × 3 mm). The peaks corresponding to gases are identified and calculated by comparing retention times with standard gases with known molar percentages of reference compounds, excluding nitrogen and water from gas composition.

2.5. Characterization of the catalysts

The acidic properties of the catalysts synthesized are examined by temperature programmed desorption (TPD) of ammonia.

Powder X-ray diffraction data (XRD) of the synthesized catalysts are collected on a Siemens D-5000 diffractometer using Cu $K\alpha_1$ radiation, using a scintillation counter. The 2θ range is from 0.5° to 10° in steps 0.017° with a sampling time of 10 s per step or from 5° to 70° in steps 0.060° with a sampling time of 1 s per step.

Nitrogen adsorption–desorption isotherms are measured at 77 K with an Autosorb Station 4 from Quantachrome, using a conventional volumetric technique. The samples are outgassed at 300 °C for 3 h.

The catalysts are also characterized by scanning electron microscopy (SEM) with a Philips XL-20 microscope and transmission electron microscopy (TEM) with a JEM-2100 (UHR) microscope.

X-ray photoelectron spectroscopy (XPS) of the samples was collected in a Kratos-XSAM 800 Multifunctional Electron Spectrometer using monochromatic Al Kα radiation. The spectrometer was equipped with a DS300 unit for data acquisition. The binding energies were referenced to the C1s peak at 284.5 eV. The software XPS Peak Processing was used to deconvolute the peaks to separate different species of the same element.

Chemisorption experiments of hydrogen for determining the active surface area, metal dispersion and metallic crystalline size of catalysts are carried out in a high-vacuum system by pulse chromatography method. Before H_2 adsorption measurement, the catalysts are treated by temperature programmed reduction (TPR) in H_2 from 373 K to 1173 K and cooled to room temperature; NiO (spectrograde) is selected as the calibrating agent. Then H_2 pulse adsorption is performed at room temperature. Gas applied at pulse adsorption equilibrium is a nitrogen and hydrogen mixture (1% volume fraction of hydrogen). The sample weight is about 0.1 g. The volume of the quantitative tube is about 5 cm^3. Active surface area, metal dispersion and metallic crystalline size are calculated based on the amount of H_2 in pulse adsorption and total consumption of hydrogen in TPR [26].

3. Results and discussion

3.1. The amount and distribution of acidic sites on parent Al-MCM-41 and Me-Al-MCM-41

The surface acidity characterized by ammonia TPD was presented in Fig. 1 and Table 1. For Al-MCM-41, it seemed that the medium and strong acidic sites were predominant. The amounts of medium and strong acid sites were 660.7 and 302.3 μmol NH_3/g, respectively, while that of weak acid site was only 66.1 μmol NH_3/g. But it is well known that Al-MCM-41 is a catalyst with mostly medium and weak acid sites, so it was conjectured that the presence of a peak at high temperature in the ammonia TPD profile might be associated with dehydroxylation of the material.

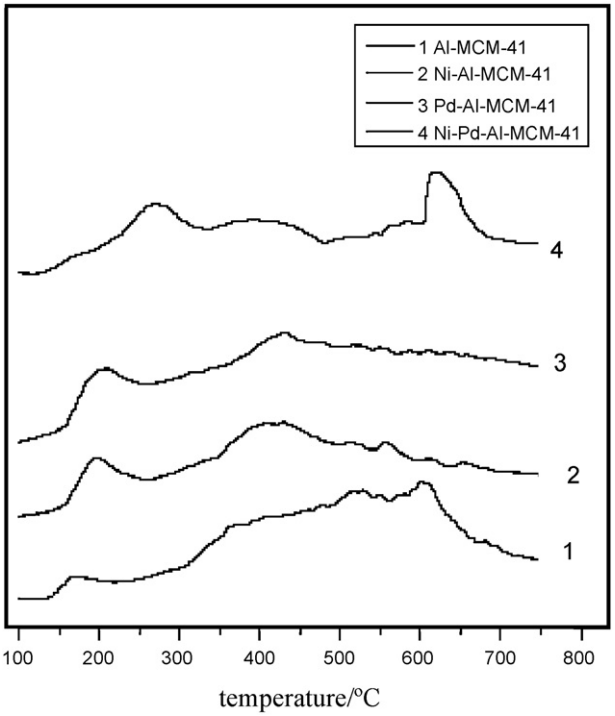

Fig. 1. Ammonia TPD profiles for (Me)-Al-MCM-41.

Table 1
Distribution of the amount and strength of acidity in (Me)-Al-MCM-41 (μmol NH_3/g).

	Weak (100–280 °C)	Medium (280–550 °C)	Strong (550–700 °C)	Total
Al-MCM-41	66.1	660.7	302.3	1029.1
Ni-Al-MCM-41	227.0	475.6	280.2	982.9
Pd-Al-MCM-41	193.3	483.9	210.4	887.6
Pd-Ni-Al-MCM-41	242.4	266.0	158.9	667.3

When nickel or palladium was introduced into Al-MCM-41 to form Me-Al-MCM-41 [20], the TPD profiles were quite different from that of Al-MCM-41. The amounts of medium and strong acid sites decreased drastically, while that of weak acid site increased significantly. When Ni and Pd were added into Al-MCM-41, an obvious weak acid site with NH_3-TPD peak temperature at about 270 °C was formed, though the strength of peaks corresponding to medium acid site become weaker. So the total amounts of weak acid site (242.4 μmol NH_3/g) came to the maximum among all catalysts, yet that of medium and strong acid sites reached to the minimum (265.9 and 158.9 μmol NH_3/g, respectively), which resulted in the minimum value of total acidic amounts (667.3 μmol NH_3/g). It was worth pointing out that when Me was introduced into the catalyst the total amounts of acidic sites decreased gradually in the following sequence: Al-MCM-41 > Ni-Al-MCM-41 > Pd-Al-MCM-41 > Ni-Pd-Al-MCM-41. In particular, for Ni-Pd-Al-MCM-41, No. 4 curve in Fig. 1 showed an emerging peak at ~650 °C, possibly indicating an increase in strong sites or the dehydroxylation of the material. The reason for the former might be in relation to the intergrowth of Ni and Pd species, which might result in the increase in strong Lewis acidic sites (seen in H_2-TPR). In conclusion, these results mentioned above might relate to the nature of metal introduced: when the catalysts Me-Al-MCM-41 were hydrothermally synthesized, Me might substitute the silicon or aluminium in the mesoporous framework of Al-MCM-41 [20,27], which resulted in the formations of some new Brønsted acidic sites [28]; in addition, the coordinatively unnaturated metals out of the mesoporous framework might act as the centers of Lewis acidic site [29].

3.2. The pore architecture, metal siting and chemisorption experiments of hydrogen of parent Al-MCM-41 and Me-Al-MCM-41

3.2.1. X-ray diffractograms at small angles

X-ray diffractograms at small angles for the synthesized samples were measured to study their pore architecture, as shown in Fig. 2. The XRD diffractogram of Al-MCM-41 exhibited low-angle reflections with *d*-values at about 38 Å (1 0 0 reflection), 22 Å (1 1 0 reflection), 19 Å (2 0 0 reflection) and 14 Å (2 1 0 reflection), respectively. The *d100* reflection was very strong and sharp, indicating a good crystallinity of mesopore structure.

When Me was introduced into catalyst Al-MCM-41, the X-ray diffractograms of Me-Al-MCM-41 were quite different from that of Al-MCM-41. For Ni-Al-MCM-41 and Pd-Al-MCM-41, although the *d100* reflection could be observed, its intensity decreased significantly, and the other three reflections merged into a low-intensity, ill-defined peak [16,20,30]. For Ni-Pd-Al-MCM-41, the combination of Ni-Pd resulted in nearly all reflections disappeared, so the change in the *d100* reflection was different from that in Refs. [16,20]. The decrease in intensity of reflection peaks from Al-MCM-41 to Me-Al-MCM-41 might be resulted from the different incorporation of metal species into the framework of materials synthesized [28]. Furthermore, the XRD diffractograms of Pd-Al-MCM-41 and Ni-Pd-Al-MCM-41 had lower intensity than that of Ni-Al-MCM-41, indicating a higher degree of damage to the mesoporous structure for the Pd and Ni-Pd containing catalysts. It had been reported

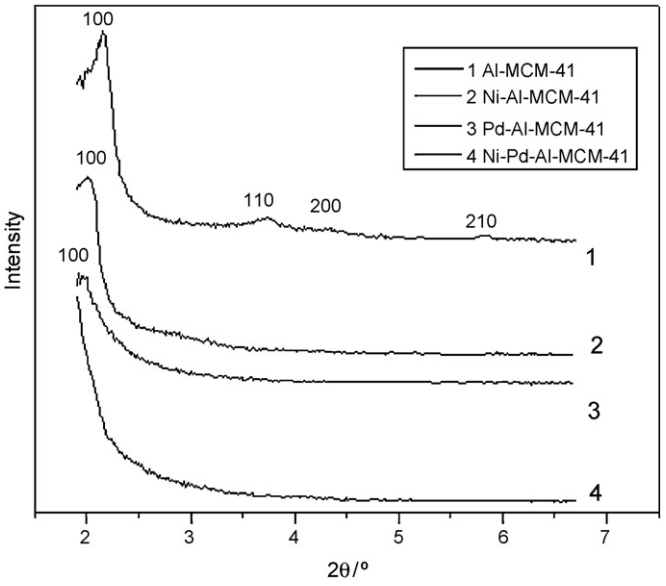

Fig. 2. XRD patterns of (Me)-Al-MCM-41 samples (at small angles).

that the long-range structural ordering would decrease to a certain degree with the incorporation of Me during the synthesis of Me-Al-MCM-41 [31], so taking it into account that the change in XRD profiles at small angles, amount and distribution of acidic sites on parent Al-MCM-41 and Me-Al-MCM-41 in this work, it was reasonable to deduce that the hexagonal arrangement of parallel mesopores was damaged with the introduction of Me in the following sequence: Ni-Pd-Al-MCM-41 > Pd-Al-MCM-41 > Ni-Al-MCM-41.

3.2.2. Analysis of N_2 adsorption–desorption isotherms

The total surface areas, pore volumes and pore sizes of the calcined mesoporous (Me)-Al-MCM-41 materials were calculated from N_2 adsorption–desorption isotherms, which results were shown in Table 2 and Fig. 3. The isotherms of catalysts synthesized were of type IV (typical of mesoporous solid) except that of Ni-Pd-Al-MCM-41, and the hysteresis loop of Ni-Pd-Al-MCM-41 was approximate to H3, yet others' were H4. It could be seen from Table 2 that the pore diameter of samples increased gradually in the following sequence Al-MCM-41 < Ni-Al-MCM-41 < Pd-Al-MCM-41 < Ni-Pd-Al-MCM-41, which suggested generally that heteroatoms incorporation would result in a shift to higher pore size [27,30]; and all of them were on a range of mesopore. On the other hand, the total pore volume decreased basically except Ni-Al-MCM-41 (the maximum of all, which might result from that Ni-Al-MCM-41 was noncrystal on the analysis of its XRD pattern (as shown in supplementary material)). As stated in Ref. [20], the type of metal was an important factor which could bring about different metal sitings and different damage to the hexagonal arrangement of parallel mesopores. In this work, it was rational to infer that, according to the results in Table 2 and Fig. 3, the pores in Ni-Pd-Al-MCM-41 were not as uniform as those in other catalysts, i.e., the damage to the hexagonal arrangement of parallel

Table 2
Pore architecture of the (Me)-Al-MCM-41materials under study.

	Total surface area (m^2 g^{-1})	Total pore volume (ml/g)	Mesopore diameter (nm)
Al-MCM-41	783	1.027	3.1
Ni-Al-MCM-41	1087	1.561	3.4
Pd-Al-MCM-41	623	1.023	3.9
Ni-Pd-Al-MCM-41	479	0.756	8.3

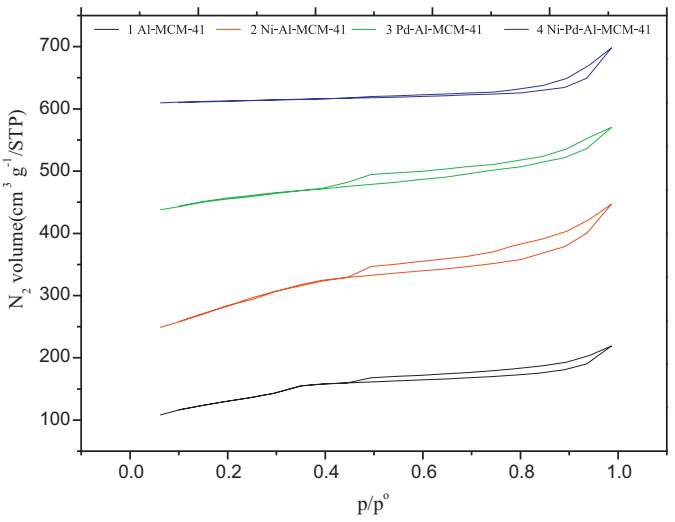

Fig. 3. Nitrogen adsorption/desorption isotherms of (Me)-Al-MCM-41 (1 Al-MCM-41, 2 Ni-Al-MCM-41: offset by 110 $cm^3\ g^{-1}$, 3 Pd-Al-MCM-41: offset by 350 $cm^3\ g^{-1}$, 4 Ni-Pd-Al-MCM-41: offset by 600 $cm^3\ g^{-1}$).

mesopores increased with the combination of the metals applied (Ni–Pd). The tendency of change in total surface area of samples was similar to that in total pore volume, which reason might also mainly relate to not only the noncrystal property of Ni-Al-MCM-41 but also the type of metal employed.

To sum up, from the results stated in Sections 3.1 and 3.2, the introduction of Me and their combination had brought about damage to the hexagonal arrangement of parallel mesopores to some extent, and the influence degree increased in the following sequence: Ni < Pd < combination of Ni and Pd. On the basis of those analysis above it was also deduced that the metal siting might be in relation to the nature of Me introduced.

3.2.3. SEM and TEM

The scanning electron microscopy (SEM) and transmission electron microscopy (TEM) images for each catalyst were shown in Figs. 4 and 5. It could be seen from Fig. 4 that the SEM of Al-MCM-41 was obviously different from those of others. It was interesting to note that many of "potato strips" were observed over Ni-Al-MCM-41, and the SEM images of Pd-Al-MCM-41 and Ni-Pd-Al-MCM-41 were similar, but the "potato strips" showed bundles, and the pore of Pd-Al-MCM-41 was more uniform than that of Ni-Pd-Al-MCM-41. It was worth mentioning that the dispersed "potato strips" over Ni-Al-MCM-41 might be related to its maximum total surface area. More interestingly, Fig. 5 displayed the fine structures of catalysts, especially for latter three catalysts, reflecting more useful information such as metal particles, metal siting and fibrous structure etc. Furthermore, it also could be observed that the "potato strips" in SEM images were composed of many fines. In addition, the SEM and TEM images of catalysts possibly confirmed the changes in amount and distribution of acidic sites and pore architecture mentioned above.

3.2.4. X-ray photoelectron spectroscopy

XPS analysis was conducted to investigate the oxidation state of the metallic atoms and their environment. A series of Ni 2p and Pd 3d XPS spectra for the Me-Al-MCM-41 catalysts were shown in

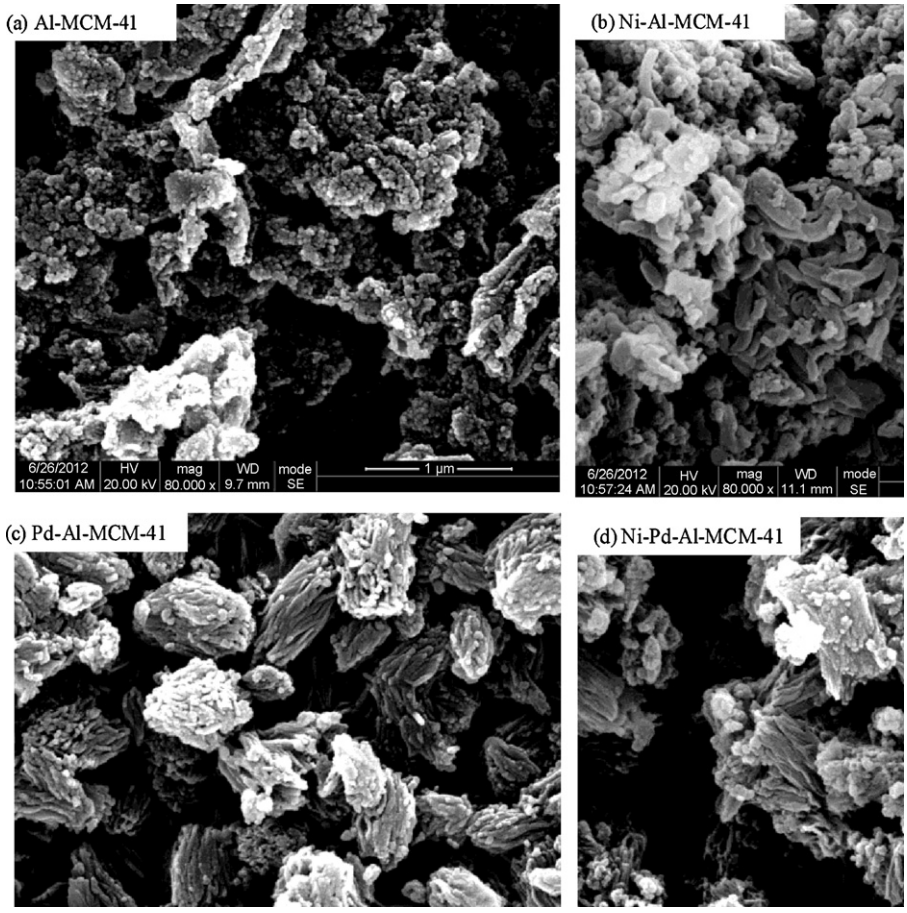

Fig. 4. SEM pictures of catalysts ((a) Al-MCM-41, (b) Ni-Al-MCM-41, (c) Pd-Al-MCM-41, (d) Ni-Pd-Al-MCM-41).

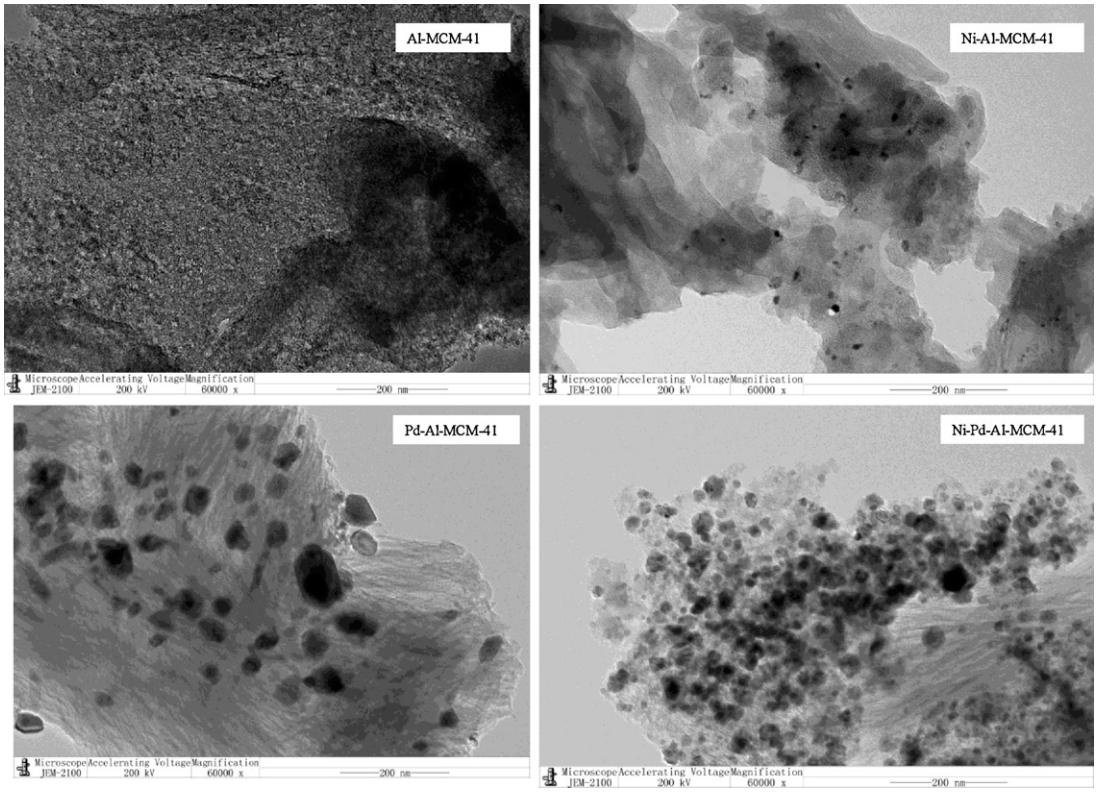

Fig. 5. TEM pictures of catalysts ((a) Al-MCM-41, (b) Ni-Al-MCM-41, (c) Pd-Al-MCM-41, (d) Ni-Pd-Al-MCM-41).

Fig. 6, and the XPS atomic surface concentrations of (Me)-Al-MCM-41 catalysts were also listed in Table 3. As shown in Fig. 6(a), the peaks at 336.7 ev (336.7 ev) and 342.1 ev (342.0 ev) were assigned to $Pd_{5/2}$ and $Pd_{3/2}$, respectively, indicating that palladium was present on the two catalysts' surface in its PdO form. Moreover, the comparison of Pd 3d in Pd-Al-MCM-41 and Ni-Pd-Al-MCM-41 in Fig. 6(a) showed that no obvious change was observed; indicating the effect of environment on both Pd-Al-MCM-41 and Ni-Pd-Al-MCM-41 was little. On the other hand, Fig. 6(b) showed that the peaks at 855.5 ev (856.1 ev) and 873.3 ev (873.9 ev) were assigned to $Ni_{3/2}$ and $Ni_{1/2}$, respectively, indicating that nickel was present on these two catalysts' surface in its NiO form; and the main two peaks of $Ni_{3/2}$ and $Ni_{1/2}$ were accompanied by a corresponding satellite peak at the higher binding energy (861.7 ev (862.2 ev) and 879.7 ev (880.1 ev), respectively). The main difference of Ni 2p in Ni-Al-MCM-41 and Ni-Pd-Al-MCM-41 was that all peaks in Ni-Pd-Al-MCM-41 had shifted to higher binding energy, which reason might lie in the influence from palladium atoms, because the electronegativity of palladium (2.2) was higher than that of nickel (1.9). In addition, differences on surface atomic concentration revealed some useful information (Table 3). Higher surface exposition of Si was observed over Al-MCM-41. On the other hand, for all synthesized samples, the surface exposition of Al was too low to be detected except Pd-Al-MCM-41 (2.2%).

Table 3
XPS atomic surface concentrations of (Me)-Al-MCM-41 catalysts.

	O (%)	Si (%)	Al (%)	Ni (%)	Pd (%)
Al-MCM-41	21.1	78.9	n.d.[a]	–[b]	–
Ni-Al-MCM-41	75.4	21.7	n.d.	3.0	–
Pd-Al-MCM-41	71.5	25.5	2.2	–	0.8
Ni-Pd-Al-MCM-41	72.7	21.2	n.d.	4.7	1.4

[a] "n.d." means "not detected" by XPS.
[b] "–" means no detection.

3.2.5. Chemisorption experiments of hydrogen

The results obtained from chemisorption experiments of hydrogen by pulse chromatography method were listed in Table 4. It could be seen that the average metallic crystalline size increased in the following sequence: Ni-Al-MCM-41 (9 nm) < Ni-Pd-Al-MCM-41 (22 nm) < Pd-Al-MCM-41 (38 nm), which might have influence on some important properties of catalysts such as active surface area, metal dispersion, etc. because the variation orders of active surface area, metal dispersion and adsorption amount of hydrogen just decreased in the following sequence: Ni-Al-MCM-41 > Ni-Pd-Al-MCM-41 > Pd-Al-MCM-41. In conclusion, on the basis of the results of characterizations such as TEM, XPS and chemisorption of hydrogen etc., the metal sitings in catalysts were described as follows: Aluminium atoms were dispersed well and basically bounded to the framework of the synthesized samples except Pd-Al-MCM-41; a part of nickel or/and Pd species in Me-Al-MCM-41 were sited in their frameworks, and the remaining ones was dispersed on their surface and inner wall of channel by nano-particles in different degree.

3.3. Catalyst evaluation under the vapor-catalyzed co-pyrolysis of LDPE and pubescens

3.3.1. Effect of (Me)-Al-MCM-41 on the yields of products

The performance of the (Me)-Al-MCM-41 samples synthesized for the co-pyrolysis process of LDPE and pubescens was presented in Table 5. In order to compare the vapor-catalyzed co-pyrolysis with the thermal co-pyrolysis, Table 5 also presented the results from thermal co-pyrolysis process. Table 5 showed that for all catalytic runs the yield of liquid and oil decreased obviously, while that of gas increased significantly in comparison to the thermal co-pyrolysis run. Antonakou et al. [16] had evaluated several types of MCM-41 in the catalytic biomass pyrolysis. The group found that a low Si/Al ratio (with more acidity) had a positive effect on product

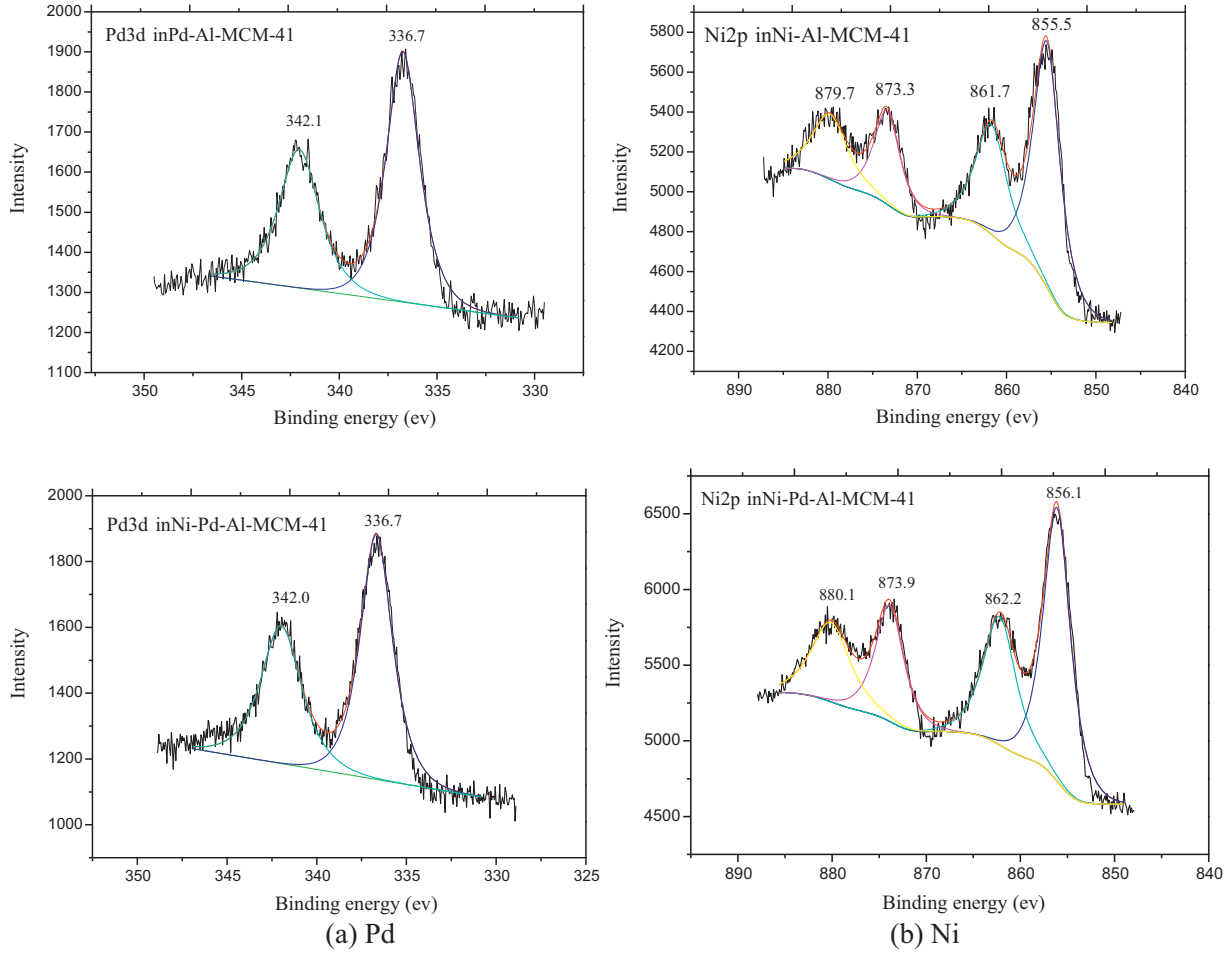

Fig. 6. X-ray photoelectron spectroscopy images of (a) Pd and (b) Ni in catalysts Ni-Al-MCM-41, Pd-Al-MCM-41 and Ni-Pd-Al-MCM-41 (offset by 500).

Table 4
Characterization results of catalysts based on the analysis of H_2 pulse adsorption.

Catalyst	Adsorption amount of H_2 (10^{-6} mol g cat^{-1})	Active surface area (m^2 g^{-1})[a]	Metal dispersion (%)[b]	Metallic crystalline size (nm)[c]
Al-MCM-41	–[d]	–	–	–
Ni-Al-MCM-41	62.3	34.4	10.8	9
Pd-Al-MCM-41	10.7	6.3	2.6	38
Ni-Pd-Al-MCM-41	18.4	10.5	4.4	22

[a] Active surface area calculated by $2 \times N_A \times$ Adsorption amount of $H_2 \times 4\pi r^2$, N_A is Avogadro constant, "r" is the metallic atomic radius ($r_{Ni} \approx 191$ pm, $r_{Pd} \approx 198$ pm)
[b] Metal dispersion calculated by $2 \times$ Adsorption amount of $H_2/2 \times$ total consumption of hydrogen in TPR
[c] Metallic crystalline size calculated by (97.1 nm)/(metal dispersion %), 97.1 nm is approximately applicable to Ni and Pd [26]
[d] "–" means no detection.

yields, and high surface areas favored the secondary cracking resulting in less liquid products. It could be seen that the results in Table 5 were both similar to and different from those in Ref. [16]. For example, the production of coke increased significantly in the presence of catalysts in Ref. [16], and yet in the present work the yield of residue seemed to remain unaffected with the presence of (Me)-Al-MCM-41 except Ni-Pd-Al-MCM-41. Furthermore, in Ref. [16] the reason for favoring the secondary cracking of the primary produced bio-oil vapors was due to the higher surface areas of the catalysts applied, yet in the work it might mainly be attributed to the acidity of catalysts. These differences might be resulted from the different raw materials and pyrolytic techniques. Chaianansutcharit et al. [19] had studied the degradations of PP/PE over aluminum-containing hexagonal mesoporous silica (Al-HMS) in a fixed bed reactor, which was very similar to our apparatus in the work. They found that Al-HMS exhibited good performance in cracking heavy molecular weight hydrocarbons into light hydrocarbons, and resulted in less oil and more gaseous products in vapor-phase-contact (VPC) reaction. It was clear that their results in relation to yield of oil and gas were similar to ours

Table 5
The influence of (Me)-Al-MCM-41 catalysts on the yield of products obtained by vapor-catalyzed co-pyrolysis (wt.%).[a]

Catalyst[b]	Liquid	Oil	Aqua	Gas	Residue
Thermal co-pyrolysis	65.5	57.9	7.7	24.4	10.1
Al-MCM-41-16cm	43.0	35.8	7.3	45.8	11.1
Ni-Al-MCM-41-16cm	53.8	45.9	7.9	34.4	11.8
Pd-Al-MCM-41–16cm	52.4	43.9	8.5	36.3	11.3
Ni-Pd-Al-MCM-41–16cm	57.4	52.0	5.4	34.3	8.3

[a] Reaction conditions: $m_{pub.}$:m_{LDPE} = 2:8, N_2 (50 mL/min), 470–450 °C, 2.5 h.
[b] The mass ratio of catalyst/reactants was 1:20.

Table 6
The influence of (Me)-Al-MCM-41 catalysts on the relative content of products in oil obtained by vapor-catalyzed co-pyrolysis (%).[a]

Catalyst[b]	Alkene	Alkane	Cycloparaffin	Aromatics
Thermal co-pyrolysis.	50.4	39.0	7.2	3.5
Al-MCM-41-16cm	19.9	56.9	10.9	12.4
Ni-Al-MCM-41-16cm	26.4	45.8	7.7	19.5
Pd-Al-MCM-41-16cm	29.1	41.1	7.0	22.4
Ni-Pd-Al-MCM-41-16cm	42.7	36.0	9.9	11.5

[a] Reaction conditions: $m_{pub.}$:m_{LDPE} = 2:8, N_2 (50 mL/min), 470–450 °C, 2.5 h.
[b] The mass ratio of catalyst/reactants was 1:20.

to a great extent. To sum up, according to all the analysis above, the explanation as to the change in yield of product in this work might be as follows: Firstly, the main reason was attributed to that vapor-catalyzed co-pyrolysis had longer retention time of gaseous pyrolytic intermediates than thermal co-pyrolysis. Secondly, the stronger acidic sites in catalysts employed mainly favored the secondary cracking of the primary pyrolytic intermediate species from the co-pyrolysis and resulted in less oil, liquid and aqua, on the contrary, more gases. Though, the effects on product yields brought about by surface areas, pore diameters of catalysts were not obvious. It should be pointed out that the change in the yield of aqua and residue from vapor-catalyzed co-pyrolysis by Ni-Pd-Al-MCM-41 was rather abnormal (to the minimum of all runs), and which reason needed discussing further later (seen in Section 3.3.5).

3.3.2. Effect of (Me)-Al-MCM-41 on the relative content of products in oil

The relative content of products in oil obtained under the vapor-catalyzed co-pyrolysis was presented in Table 6. As could be seen from it, all catalysts except Ni-Pd-Al-MCM-41 exerted strong effect of alkanisation on the primary intermediate species from the pyrolysis of LDPE, as in VPC reactions except with Ni-Pd-Al-MCM-41 the alkane/alkene ratio increased significantly in comparison with that under the thermal co-pyrolysis, the effect of alkanisation over Al-MCM-41 was the most prominent among all catalysts. It was justified to infer that the pore architecture of Al-MCM-41 and (Me)-Al-MCM-41 containing single Me strongly favored the reactions in relation to alkanisation, because the results in Table 2 demonstrated that all catalysts except Ni-Pd-Al-MCM-41 had similar average mesopore diameters.

Making a comparison between Fig. 7(a) and (b), it was very easy to observe the change in relative content of alkene and alkane in oil. First, an explanation was given as follows: the double peaks in Fig. 7(a) corresponded to alkene (left) and alkane (right) with the same carbon atoms, respectively. Then it could be seen clearly from Fig. 7(b) that under the vapor-catalyzed co-pyrolysis condition the intensity of peaks corresponding to the alkenes in oil decreased so significantly that some of them disappeared almost.

Table 6 also showed that no obvious change in the relative content of cycloparaffin from the VPC reactions was observed in comparison with that from thermal co-pyrolysis. But it exhibited that the relative content of aromatics increased to some extent under VPC conditions, especially over Ni-Al-MCM-41 and Pd-Al-MCM-41, so it could be deduced that the VPC reactions with the Al-MCM-41 and (Me)-Al-MCM-41 catalysts favored the formation of aromatics, i.e., Al-MCM-41 and (Me)-Al-MCM-41 exerted a strong aromatization effect on the intermediate species from the pyrolysis of LDPE under VPC conditions. In addition, a comparison between the relative contents of products over Pd-Al-MCM-41 and Ni-Pd-Al-MCM-41 discovered that the combination of different metals might bring about the change of catalysis in intensity or create some new catalytic performance.

3.3.3. Effect of (Me)-Al-MCM-41 on the relative content of products in aqua

The relative content of products in aqua obtained under the vapor-catalyzed co-pyrolysis was presented in Table 7. Drawing a comparison between the relative content of phenols in aqua in Table 7 and that of aromatics in Table 6, generally it was found that, under the vapor-catalyzed conditions, if the relative content of phenols was higher, that of aromatics in corresponding oil was lower. So it was reasonable to consider that there might be some undefined interactions between the pyrolytic intermediate species from the co-pyrolysis. For Al-MCM-41, the hexagonal arrangement of parallel mesopores and strong acidity might be responsible for the effect of alkanisation on the intermediate species from the pyrolysis of LDPE and the formation of many phenolic compounds. For Ni-Al-MCM-41 and Pd-Al-MCM-41, similar pore architecture and acidity made contributions to producing a large amount of acetic acid. As to Ni-Pd-Al-MCM-41, its unique pore architecture, the effect of metal combination and acidity had brought about together its unique performance existing in the co-pyrolysis. For example, the yield of aqua shown in Table 5 was only 5.4% (the minimum in all runs), the relative content of acetic acid in Table 7 was only 22.5% (the minimum in all runs) and the relative content of phenols in Table 7 reached to 44.7% (the maximum in all runs) etc.

3.3.4. Effect of (Me)-Al-MCM-41 on the composition of gases

The molar composition of gases from the co-pyrolysis of LDPE and pubescens was presented in Table 8. As shown in Table 8, (Me)-Al-MCM-41 exhibited stronger ability to produce hydrogen than Al-MCM-41. The ability to produce hydrogen increased in the following sequence: Pd-Al-MCM-41 (17.0 vol.%)< Ni-Al-MCM-41 (24.9 vol.%)< Ni-Pd-Al-MCM-41 (61.8 vol.%). It was clear that the sum of 17.0 vol.% and 24.9 vol.% was less than 61.8 vol.%, which strongly indicated that the combination of Ni and Pd in Ni-Pd-Al-MCM-41 had resulted in strong synergistic effect of producing hydrogen, as well as significant decrease in the yield of other gases such as CO, CH_4, C_4H_8. Nickel-based catalysts had been prepared and investigated for their suitability for the production of hydrogen from materials related to biomass [31–37] and plastics [4,38,39]. The deactivation of nickel-based catalysts was caused usually by nickel sintering and carbon deposition, so many researchers had tried to improve their properties by introducing some metals such as magnesium, lanthanum, cobalt and chromium [33], etc. or using different preparation methods. The reason for this was that magnesium and lanthanum could enhance steam adsorption to facilitate the gasification of coke precursors and cobalt and chromium could slow down the surface reactions leading to the formation of the coke precursors. In the present work the introduction of Pd into Ni-Al-MCM-41 altered many properties in Ni-Pd-Al-MCM-41 to a great extent, in comparison with those in Ni- or Pd-Al-MCM-41, such as acidity, pore volume and pore diameter as well as catalytic performance. Moreover, compared to the operating temperature applied in other works of producing hydrogen from biomass or plastics, it was worth mentioning that the reaction temperature in this work was only in the range of 450–470 °C, so Ni-Pd-Al-MCM-41 might play its special application in development of hydrogen energy, exploitation and utilization of biomass as well as solid wastes such as waste plastics, etc.

According to the results obtained above, it was also rational to infer that, as demonstrated in Ref. [20], the type of metal was of more importance than the metal siting, although the pore structure, the siting and type of metal in catalyst also affected the catalytic properties of (Me)-Al-MCM-41.

3.3.5. Scheme of reactions

On the one hand, in order to follow what were happening in the reaction medium, reaction pathways involved of intermediates

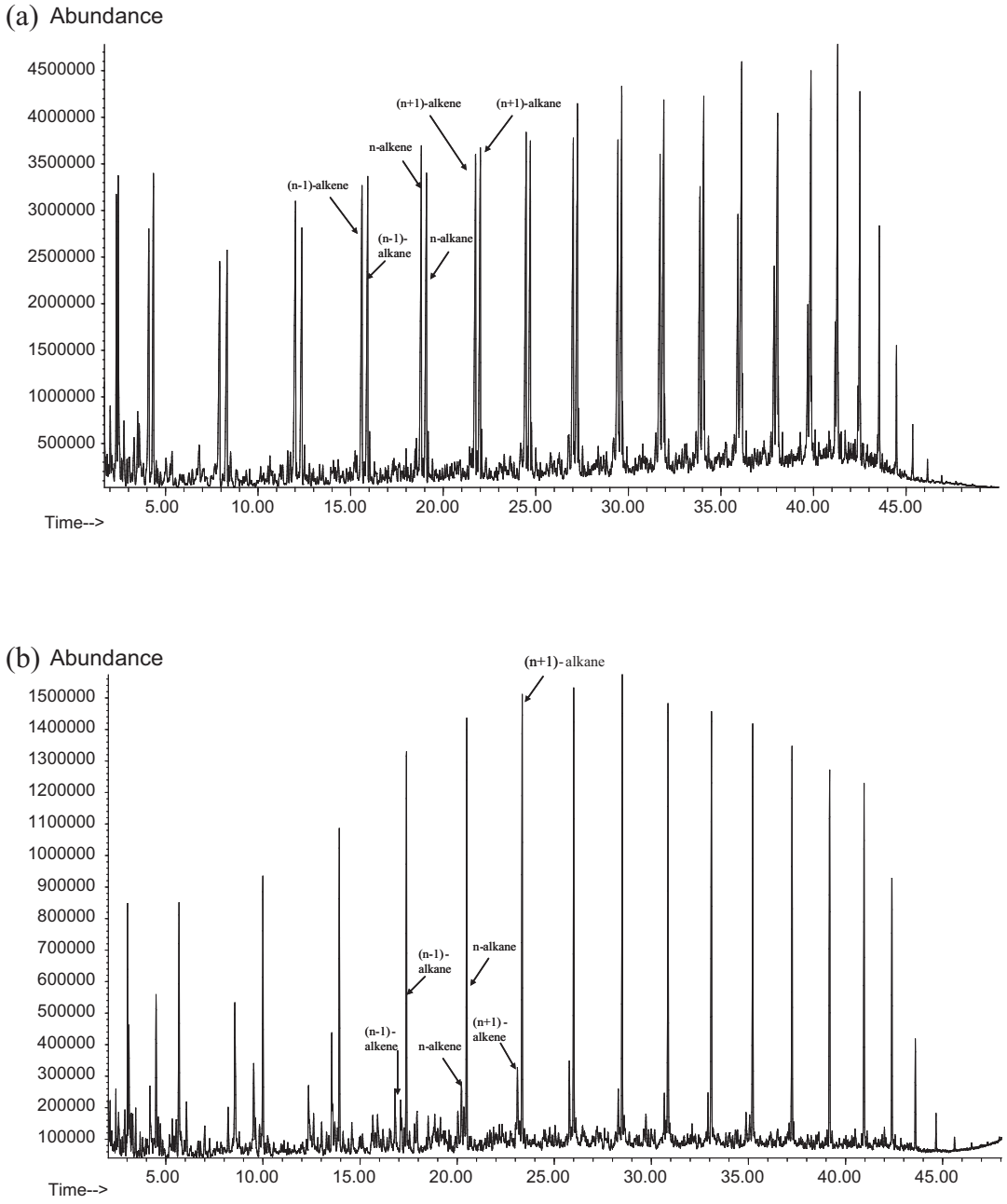

Fig. 7. GC–MS chromatograms of products in oil under different co-pyrolysis.
(a) The total ion chromatograms of products in oil obtained by thermal co-pyrolysis
(b) The total ion chromatograms of products in oil obtained by vapor-catalyzed co-pyrolysis over Ni-Al-MCM-41.

Table 7
The influence of (Me)-Al-MCM-41 catalysts on the relative content of products in aqua obtained by vapor-catalyzed co-pyrolysis (%).[a]

Catalyst[b]	Acetic acid	Acid–ester[c]	Ald.–ket[d]	Furans	Phenols	Others
Thermal co-pyrolysis	36.8	10.4	14.7	7.8	26.9	3.4
Al-MCM-41-16cm	55.8	4.1	1.6	3.1	30.3	5.2
Ni-Al-MCM-41-16cm	84.6	3.0	4.1	n.d.[e]	7.9	0.4
Pd-Al-MCM-41-16cm	86.7	3.1	2.8	0.4	6.5	0.6
Ni-Pd-Al-MCM-41-16cm	22.5	10.0	13.9	1.0	46.7	5.9

[a] Reaction conditions: $m_{pub.}$:m_{LDPE} = 2:8, N_2 (50 mL/min), 470–450 °C, 2.5 h.
[b] The mass ratio of catalyst/reactants was 1:20.
[c] Other carboxylic acid and ester.
[d] Aldehyde and ketone.
[e] "n.d." Indicates that no corresponding substance was observed or detected.

Table 8
Composition of gases from the co-pyrolysis of LDPE and pubescens (vol.%).[a]

	H_2	CO	CH_4	CO_2	C_2H_4	C_2H_6	C_3H_6	C_3H_8	C_4H_8	C_4H_{10}
Pyrolysis[b]	8.2	10.3	22.6	7.1	7.1	11.3	6.4	11.2	7.6	8.2
Thermal co-pyrolysis	6.1	8.9	21.2	15.0	7.1	12.9	7.3	10.2	3.5	7.9
Al-MCM-41-16cm[c]	4.9	7.1	17.7	10.2	5.0	8.3	23.6	5.5	9.0	8.7
Ni-Al-MCM-41-16cm[c]	24.9	11.9	26.5	6.7	9.0	9.6	3.7	2.4	2.4	2.8
Pd-Al-MCM-41-16cm[c]	17.0	11.0	28.2	7.7	10.6	11.0	5.2	2.7	2.6	4.1
Ni-Pd-Al-MCM-41-16cm[c]	61.8	1.2	1.8	8.0	6.5	7.0	6.6	4.3	n.d.[d]	2.9

[a] Reaction conditions: $m_{pub.}$:m_{LDPE} = 2:8, N_2 (50 mL/min), 470–450 °C, 2.5 h.
[b] The gaseous mixture made up of the gas from thermal pyrolysis of pubescens, LDPE, respectively.
[c] The mass ratio of catalyst/reactants was 1:20.
[d] "n.d." means "not detected".

over catalysts (taking Ni-Pd-Al-MCM-41 as an example) during vapor-catalyzed condition were proposed (seen in Scheme 1) on the base of the results in Tables 5–8. Firstly, according to the common views, under vapor-catalyzed co-pyrolysis condition the carbonium ions from the pyrolysis of LDPE formed by acidic sites over catalysts underwent easily cyclization reactions resulting in the formation of aromatics as well as hydrogen. The relative contents of aromatics under vapor-catalyzed condition in Table 6 just proved this speculation. Secondly, lots of steam reforming reactions happened during the course of vapor-catalyzed co-pyrolysis [40]. It had been reported that both acetic acid and alcohol could react with steam for hydrogen production [41–44], while other products such as methane and carbon oxide, etc. were obtained. Both the yield of aqua, residue in Table 5 and the relative content of acetic acid in Table 7 were the minimum (5.4%, 8.3% and 22.5%, respectively), which justified that not only acetic acid could react with steam but also the ability of steam reforming over Ni-Pd-Al-MCM-41 was most prominent under the condition, which facilitated the gasification or slowed down the formation of coke precursors [33]. In addition, aromatics might react with steam resulting in the higher yields of phenols (46.7%, seen in Table 7) and hydrogen. In a word, the two kinds of reaction pathways just mentioned above might be responsible for the highest yield of hydrogen (61.8%, vol.%). It was worth pointing out that the steam reforming reactions were not prominent over Ni-Al-MCM-41 and Pd-Al-MCM-41. Thirdly, there might be some complex interactions between the intermediates from the co-pyrolysis. As shown in Scheme 1, it was speculated that acetic acid could react with alcohol so as to form esters, and benzene might react with acetic acid to form phenol and aldehyde. These speculations were in good accordance with the corresponding results in Table 7.

On the other hand, the information displayed by the H_2-TPR profiles of catalysts was very valuable, by which the mechanism of synergistic effect of producing hydrogen over Ni-Pd-Al-MCM-41 might be revealed. As shown in Fig. 8, the NiO species over Ni-Al-MCM-41 were most difficultly reduced among the three catalysts, because when NiO species over Ni-Al-MCM-41 were reduced fully, the temperature needed to reach 850 °C nearly. But it was clearly observed that the PdO over Pd-Al-MCM-41 was greatly easier to be reduced than NiO over Ni-Al-MCM-41. More interestingly, when Pd was introduced into the system of Ni-Pd-Al-MCM-41 catalyst, both NiO and PdO could be reduced totally at about 650 °C. In addition, two pairs of double shoulder peaks were observed at about 180 °C and 350 °C, respectively. Which reason might be deduced as follows: first, as stated in Section 3.1, the intergrowth of Ni and Pd species might result in the increase in strong Lewis acidic sites over Ni-Pd-Al-MCM-41. On the basis of the electronegativity (palladium (2.2), nickel (1.9)), it was deduced that Ni species should be responsible mainly for the increase in acidity; in other word, the oxidative ability of Ni species was enhanced by the intergrowth

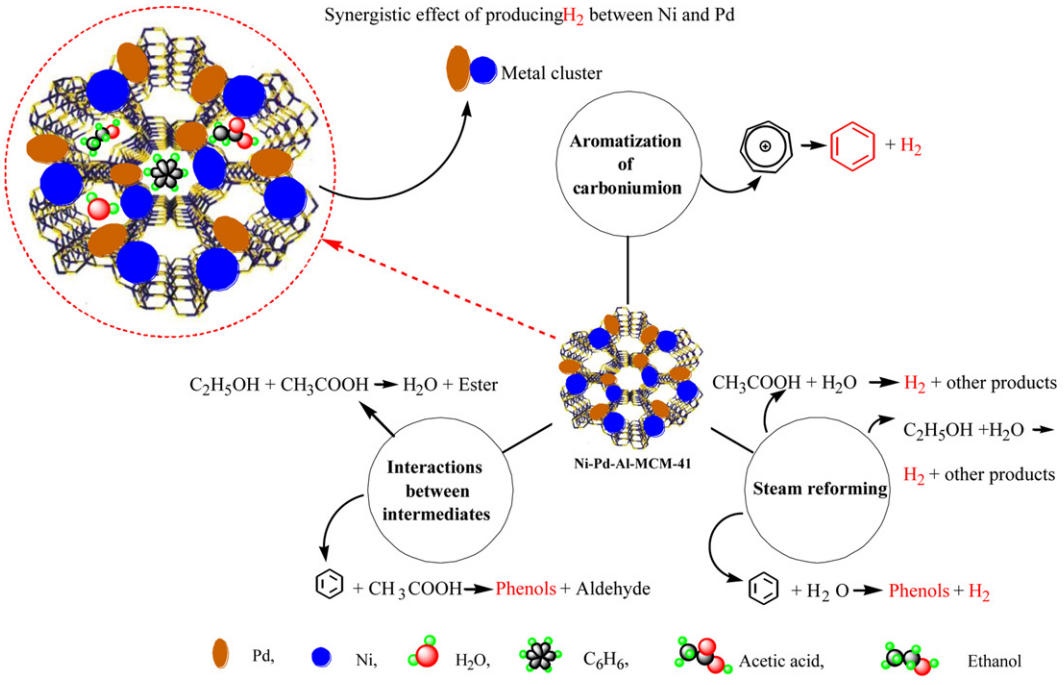

Scheme 1. Reaction pathway of intermediates over Ni-Pd-Al-MCM-41 during vapor-catalyzed condition.

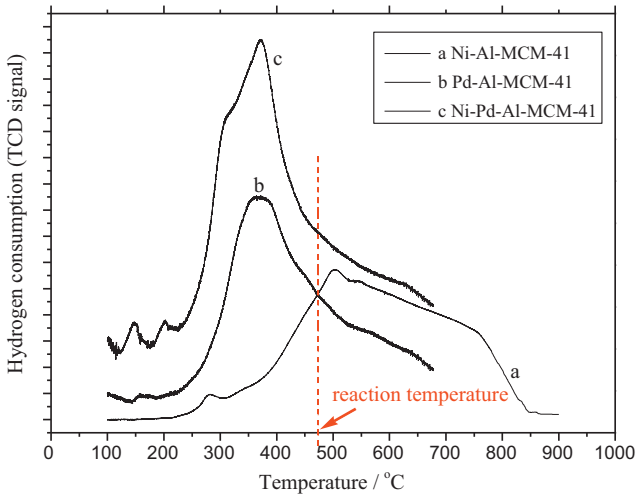

Fig. 8. H_2-TPR profiles of catalysts ((a) Ni-Al-MCM-41, (b) Pd-Al-MCM-41, (c) Ni-Pd-Al-MCM-41).

[45]. Furthermore, when PdO was reduced into Pd first, Pd might adsorb hydrogen, so the hydrogen absorbed by Pd might promote the reduction of NiO to a certain extent. Just because of the facts mentioned above, the mechanism of synergistic effect of producing hydrogen over Ni-Pd-Al-MCM-41 might be explained as follows: first, under the experimental conditions (the dotted line in Fig. 8 indicated the reaction temperature) most of NiO and PdO over Ni-Pd-Al-MCM-41 were reduced into metal atoms. Second, as shown in Table 8, Ni atoms over Ni-Al-MCM-41 had a stronger ability to produce hydrogen than Pd atoms over Pd-Al-MCM-41, so catalyst Ni-Pd-Al-MCM-41 produced a larger amount of hydrogen under the same condition than Ni-Al-MCM-41 and Pd-Al-MCM-41. As regards the reason resulting in the stronger producing hydrogen of Ni atoms, it was conjectured that Ni atoms promoted the steam reforming reactions mentioned above than Pd, i.e., these reactions were favored greatly by Ni atoms over Ni-Pd-Al-MCM-41 so as to produce more hydrogen. Moreover, it could not be neglected that the intermediates from the pyrolysis of LDPE might undergo a series of dehydrogenation over Ni-Pd-Al-MCM-41 (as shown in Table 6, for Ni-Pd-Al-MCM-41, the ratio of alkane to alkene was the minimum among all vapor-catalyzed co-pyrolysis), which had also made contribution to the high yield of hydrogen (61.8 vol.%).

4. Conclusions

Several hydrothermally synthesized catalysts (Me)-Al-MCM-41 were characterized and applied in the vapor-catalyzed co-pyrolysis of pubescens and LDPE. The results suggested that:

(1) The incorporation of Me into Al-MCM-41 had brought about some changes in structure of (Me)-Al-MCM-41 to a certain degree such as surface area, pore volume, pore diameter and hexagonal arrangement etc. The influence increased in the following sequence: Ni < Pd < combination of Ni and Pd.
(2) Results based on the vapor-catalyzed co-pyrolysis over (Me)-Al-MCM-41, especially for Ni-Pd-Al-MCM-41, showed that the intermediates containing benzene ring might react with other intermediates with hydroxyl such as water molecule, alcohol and carboxylic acid etc., resulting in the formation of phenolic compounds, hydrogen and other products. So the relative content of aromatics in oil was higher, whereas that of phenol in corresponding aqua was lower, and vice versa; and these facts supported the view that there were some interactions between the intermediate species from the co-pyrolysis.
(3) The results also showed that the type of metal was of more importance than the metal siting. The combination of Ni with Pd might result in a novel performance during the co-pyrolysis. The synergistic effect on producing hydrogen, probably resulting from not only the promotion of Pd to Ni species but also the strong ability of Ni as well as Pd to produce hydrogen, declared that Ni-Pd-Al-MCM-41 had great potential of hydrogen production, which implied that the catalyst might play its special application in development of hydrogen energy, exploitation and utilization of biomass as well as municipal solid waste such as waste plastics, etc.

Acknowledgements

This work was financially supported by the National Basic Research Program of China (973 program, No. 2007CB210203), and the Special Research Fund for the Doctoral Program of Higher Education of China (No. 20050610013).

Appendix A. Supplementary data

Supplementary data associated with this article can be found, in the online version, at http://dx.doi.org/10.1016/j.apcatb.2012.09.002.

References

[1] A. López, I. de Marco, B.M. Caballero, M.F. Laresgoiti, A. Adrados, A. Aranzabal, Applied Catalysis B 104 (2011) 211–219.
[2] A. Marcilla, A. Gómez-Siurana, J.C. García Quesada, D. Berenguer, Journal of Analytical and Applied Pyrolysis 85 (2009) 327–333.
[3] G. Elordi, M. Olazar, G. Lopez, P. Castaño, J. Bilbao, Applied Catalysis B 102 (2011) 224–231.
[4] C.F. Wu, Paul T. Williams, Applied Catalysis B 90 (2009) 147–156.
[5] A. Pattiya, J.O. Titiloye, A.V. Bridgwater, Fuel 89 (2010) 244–253.
[6] H. Lee, H.J. Park, Y.K. Park, J.Y. Hur, J.K. Jeon, J.M. Kim, Catalysis Today 132 (2008) 68–74.
[7] M. Brebu, S. Ucar, C. Vasile, J. Yanik, Fuel 89 (2010) 1911–1918.
[8] A. Caglar, B. Aydinli, Journal of Analytical and Applied Pyrolysis 86 (2009) 304–309.
[9] C.Q. Dong, Y.P. Yang, B.S. Jin, M. Horio, Waste Management 27 (2007) 1557–1661.
[10] P. Rutkowski, A. Kubacki, Energy Conversion and Management 47 (2006) 716–731.
[11] V.I. Sharypov, N.G. Beregovtsova, B.N. Kuznetsov, S.V. Baryshnikov, V.L. Cebolla, J.V. Weber, S. Collura, G. Finqueneisel, T. Zimny, Journal of Analytical and Applied Pyrolysis 76 (2006) 265–270.
[12] V.I. Sharypov, N.G. Beregovtsova, B.N. Kuznetsov, L. Membrado, V.L. Cebolla, N. Marin, J.V. Weber, Journal of Analytical and Applied Pyrolysis 67 (2003) 325–340.
[13] E.F. Iliopoulou, E.V. Antonakou, S.A. Karakoulia, I.A. Vasalos, A.A. Lappas, K.S. Triantafyllidis, Chemical Engineering Journal 134 (2007) 51–57.
[14] V. Parvulescu, C. Anastasescu, C. Constantin, B.L. Su, Catalysis Today 78 (2003) 477–485.
[15] V. Pârvulescu, C. Anastasescu, B.L. Su, Journal of Molecular Catalysis A: Chemical 211 (2004) 143–148.
[16] E. Antonakou, A. Lappas, M.H. Nilsen, A. Bouzga, M. Stöcker, Fuel 85 (2006) 2202–2212.
[17] J. Adam, M. Blazsó, E. Mészáros, Mi Stöcker, M.H. Nilsen, A. Bouzga, J.E. Hustad, M. Grønli, Fuel 84 (2005) 1494–1502.
[18] J. Adam, E. Antonakou, A. lappas, M. Stöcker, M.H. Nilsen, A. Bouzga, J.E. Hustad, G. Øye, Microporous and Mesoporous Materials 96 (2006) 93–101.
[19] S. Chaianansutcharit, R. Katsutath, A. Chaisuwan, T. Bhaskar, A. Nigo, A. Muto, Y. Sakata, Journal of Analytical and Applied Pyrolysis 80 (2007) 360–368.
[20] M.H. Nilsen, E. Antonakou, A. Bouzga, A. Lappas, K. Mathisen, M. Stöcker, Microporous and Mesoporous Materials 105 (2007) 189–203.
[21] S.M. Jin, K.X. Cui, H.Y. Guan, M. Yang, L. Liu, C.F. Lan, Applied Clay Science 56 (2012) 1–6.
[22] S. Stephanidis, C. Nitsos, K. Kalogiannis, E.F. Iliopoulou, A.A. Lappas, K.S. Triantafyllidis, Catalysis Today 167 (2011) 37–45.
[23] A. Marcilla, M. Beltran, A. Gómez-Siurana, I. Martinez, D. Berenguer, Thermochimica Acta 518 (2011) 47–52.
[24] C. Torri, I.G. Lesci, D. Fabbri, Journal of Analytical and Applied Pyrolysis 85 (2009) 192–196.
[25] W.W. Liu, C.W. Hu, Y. Yang, D.M. Tong, G.Y. Li, L.F. Zhu, Energy Conversion and Management 51 (2010) 1025–1032.
[26] T. Miyazawa, T. Kimura, J. Nishikawa, S. Kado, K. Kunimori, K. Tomishige, Catalysis Today 115 (2006) 254–262.

[27] Y. Kong, S.Y. Jiang, J. Wang, S.S. Wang, Q.J. Yan, Y.N. Lu, Microporous and Mesoporous Materials 86 (2005) 191–197.
[28] R. Tismanneanu, B. Ray, R. Khalfin, R. Semiat, M.S. Eisen, Journal of Molecular Catalysis A: Chemical 171 (2001) 229–241.
[29] A. Corma, M.T. Navarro, M. Renz, Journal of Catalysis 219 (2003) 242–246.
[30] M. Selvaraj, A. Pandurangan, K.S. Seshadri, P.K. Sinha, K.B. Lal, Applied Catalysis A 242 (2003) 347–364.
[31] Z. Luan, H.Y. He, W. Zhou, C.F. Cheng, J. Klinowski, Journal of the Chemical Society, Faraday Transactions 91 (1995) 2955.
[32] K. Bru, J. Blin, A. Julbe, G. Volle, Journal of Analytical and Applied Pyrolysis 58 (2006) 59–63.
[33] L. Garcia, R. French, S. Czernik, E. Chornet, Applied Catalysis A 201 (2000) 225–239.
[34] C.F. Wu, L.Z. Wang, P.T. Williams, J. Shi, J. Huang, Applied Catalysis B 108–109 (2011) 6–13.
[35] Q.L. Hao, C. Wang, D.Q. Lu, Y. Wang, D. Li, G.J. Li, International Journal of Hydrogen Energy 35 (2010) 8884–8890.
[36] S.Y. Zhang, X.J. Wang, J.P. Cao, T. Takarada, Bioresource Technology 102 (2011) 2033–2039.
[37] M. Zhao, N.H. Florin, A.T. Harris, Applied Catalysis B 92 (2009) 185–193.
[38] C.F. Wu, P.T. Williams, Applied Catalysis B 87 (2009) 152–161.
[39] J.M. Escola, J. Aguado, D.P. Serrano, A. García, A. Peral, L. Briones, R. Calvo, E. Fernandez, Applied Catalysis B 106 (2011) 405–415.
[40] D.L. Li, L. Wang, M. Koike, Y. Nakagawa, K. Tomishige, Applied Catalysis B 102 (2011) 528–538.
[41] A. Haryanto, S. Fernando, N. Murali, S. Adhikari, Energy and Fuels 19 (2005) 2098–2106.
[42] K. Takanabe, K. Aika, K. Seshan, L. Lefferts, Chemical Engineering Journal 120 (2006) 133–137.
[43] F. Bimbela, D. Chen, J. Ruiz, L. García, J. Arauzo, Applied Catalysis B 119-120 (2012) 1–12.
[44] G. Guan, G. Chen, Y. Kasai, E. Wee, C. Lim, X. Hao, M. Kaewpanha, A. Abuliti, C. Fushimi, A. Tsutsumi, Applied Catalysis B 115-116 (2012) 159–168.
[45] G. Berlier, E. Gribov, D. Cocina, G. Spoto, A. Zecchina, Journal of Catalysis 238 (2006) 243–249.